MarsExpress ASPERA-3
NPD FM2 calibration report (draft)

A. Grigoriev, S. Barabash, A. Fedorov

March 18, 2003

MEX NPD FM2

–> NPD flight model 2 developed for MarsExpress mission ASPERA-3 experiment

–> Calibrated 020105

–> Launch date 020505 (lauched to Mars)

–> Installed into ASPERA-3 close to DPU box and will be considered as NPD1 in future while instrument commanding and data analysis.

–> Is complemented by NPD FM3 (NPD SPARE model) which is to be considered as NPD2 in future while instrument commanding and data analysis

NPD sensor general description

Neutral Particle Detector (NPD) developed for the ESA Mars Express mission is a compact low weight (650g) high efficiency sensor to image low energy neutral atoms (ENA) resulted from the solar wind interaction with the Martian exosphere. NPD provides measurements of the ENA differential flux over the energy range 100 eV - 10 keV resolving H and O with a coarse $5 \times 30^{\circ}$ angular resolution and total efficiency $1 - 50\%$. The sensor consists of two identical detectors each with a 9 $\times$ 90 $^{\circ}$ intrinsic field of view placed on a scanning platform which performs 180° scans to cover a hemisphere. The measurement principle is based on surface interaction technique.

Principle design of the NPD sensor, see Figure 1

ENAs incident on a start surface at a grazing angle of 15° are reflected under approximately a mirror angle and cause secondary electron emission in the StartSurface. The secondary electrons are transported to an Start MCP assembly, which gives the START signal. The reflected ENAs hit the stop surface and again produce the secondary electrons used to generate the STOP signal in the Stop MCP assembly. The Time-of-Flight measurements give ENA velocity, the STOP signal is also used to identify mass (H or O). Coincidence technique as well as properties of the START and STOP surface coating provide UV suppression to the level sufficient to achieve the required signal-to-noise ratio.

1 NPD calibration setup. Coordinate system. Technical details.

1.1 Technical details

As it is seen on the Figure 1, the sensor has 3 detectors in the azimuthal plane. The detectors direction definition is presented on the Fig. 2. The basic position of the NPD sensor, integrated

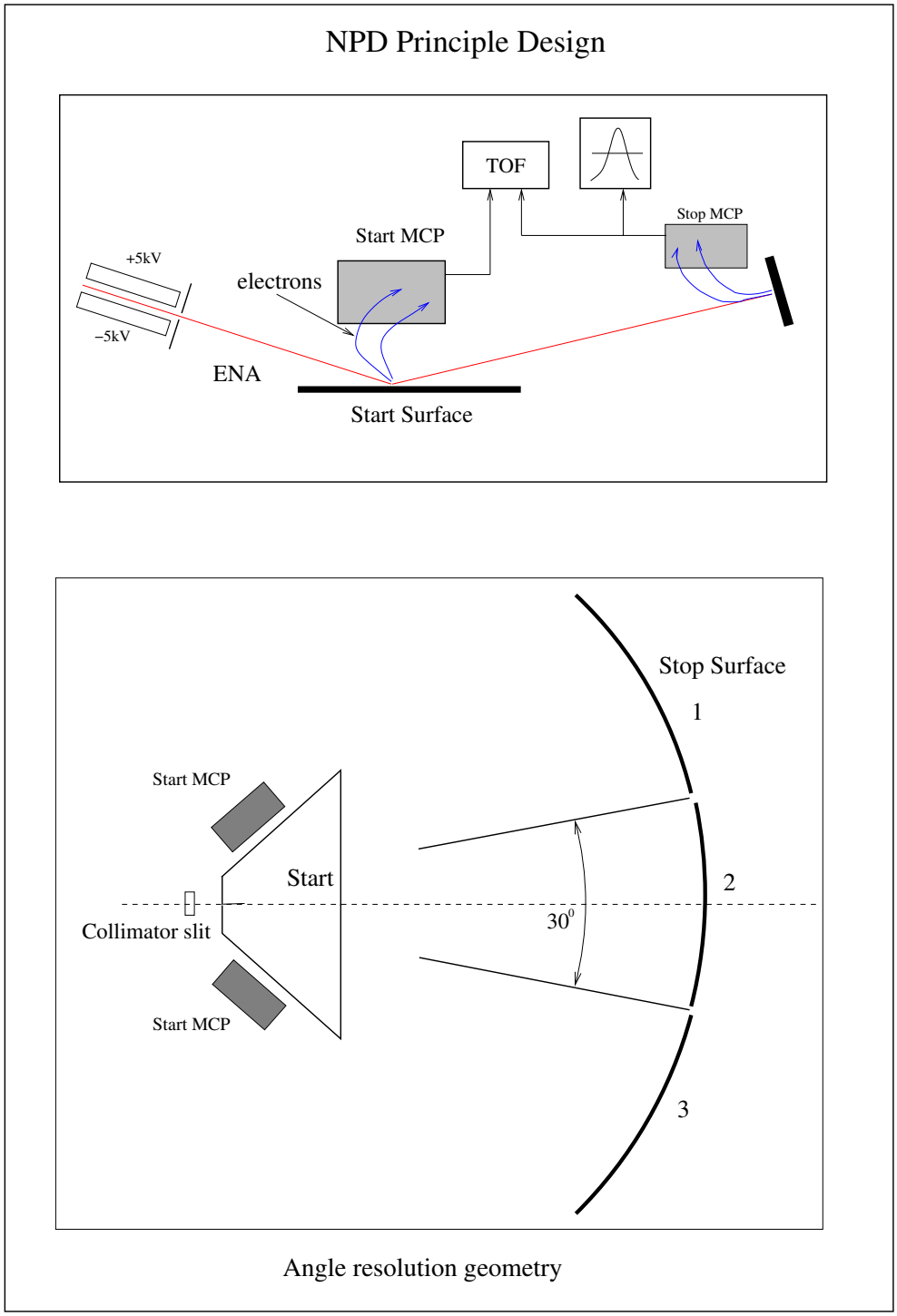

Figure 1: The principle design of NPD sensor.

with ASPERA-3 is such, that its long side is placed in the horizontal plane, along the scanner platform. While scanning it will scan in the NPD's elevation plane.

Figure 2 describes the directions of view of each of NPD detectors. The "zero" direction is set to correspond to the detector placed in the vertical plane, which is along the short side of the chassi. The direction 2 corresponds to the detector placed in the horizontal plane with the pinhole position. The detector 1 is the detector in-between the 0 one and the number 2.

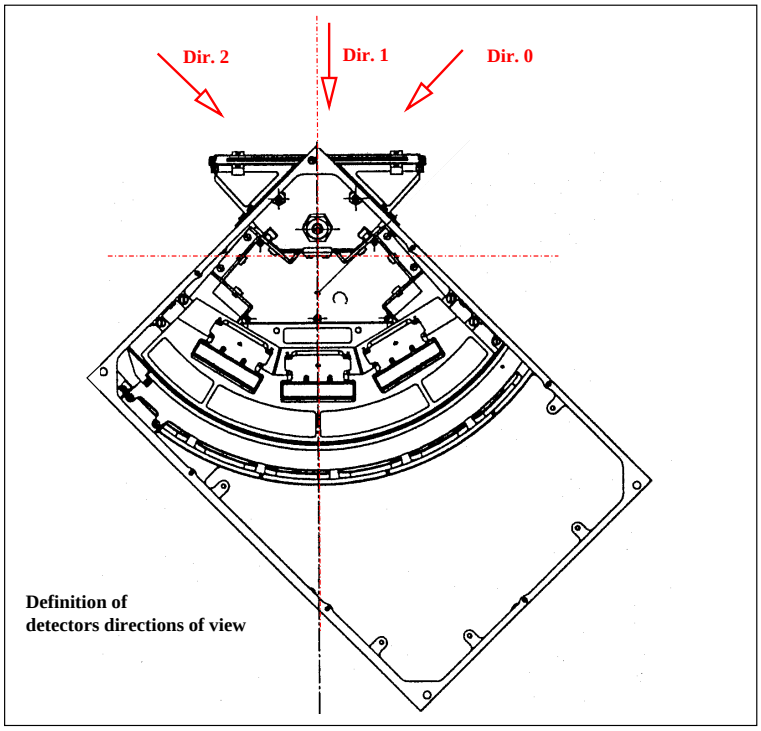

Figure 2: The Instrument directions definition.

The cross-section of the sensor along the plane "pinhole – Detector 1" is shown on Figure 3. The deflector is declined on $15°$ from the StartSurface plane. The incoming beam comes though the collimator slit, between deflector electrodes, through a pinhole and incident on a StartSurface. The collimator slit has dimensions $4.5 \times 70.0mm^2$. The distance between deflector electrodes is $4.5mm$. They are biased with $+/-5kV$ to deflect charged particles with energy less than the deflector energy cut-off 60 keV. Deflector provides field of view of the sensor $9° \times 90°$. Pinhole has dimensions $3.0 \times 4.5mm^2$. On the sensor cross-section on the Figure 3 Deflector, StartSurface, StopSurface and the middle Stop MCP detector are clearly seen.

1.2 Calibration facilities

There will be some facts about the Calibration Facility used to calibrate NPD

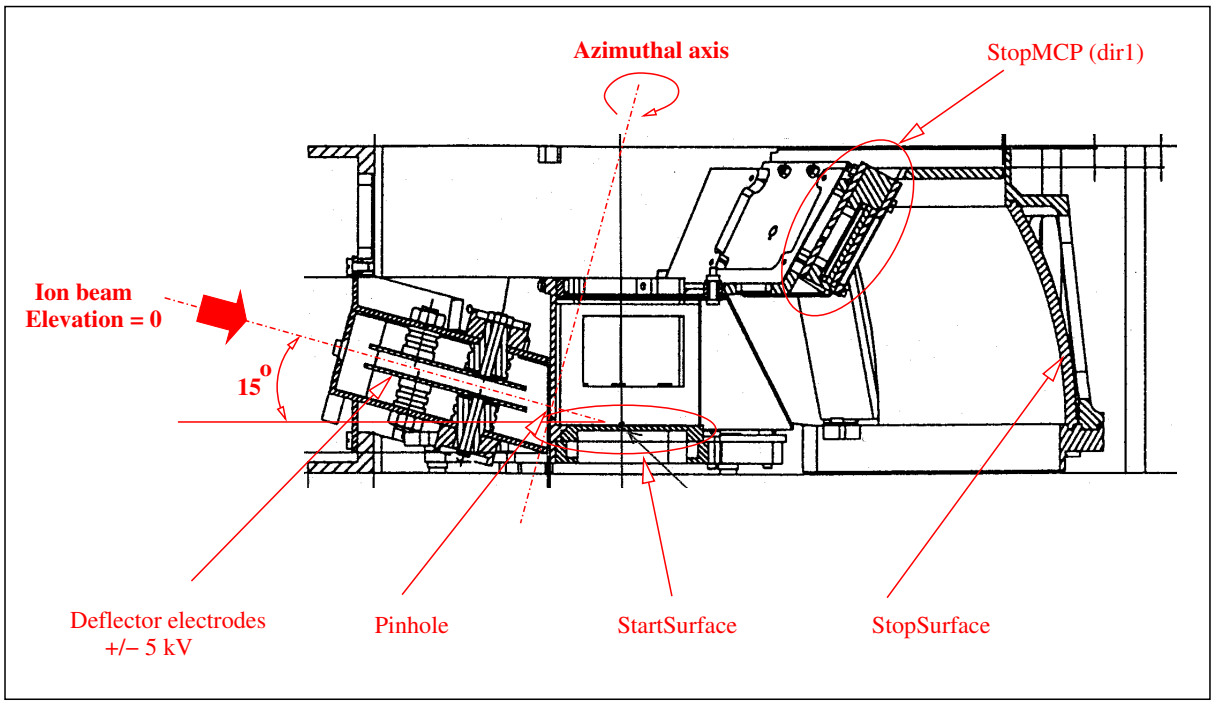

Figure 3: The Instrument's cross section.

1.3 Calibration set up

Sensor has been calibrated in stand-alone configuration.
On the Figure 4 NPD calibration mechanical set up is shown. NPD is placed in the vacuum chamber on the turntable at the distance $\sim 1.7m$ from the output aperture of the ion beam source. It can be sweeped in both azimuthal and elevation directions in the wide range of angles, $> 90°$ in both directions with an accuracy at least $1°$. Also the turntable can be displaced across the incident beam in the perpendicular directions (vertical and horizontal ones) to align the sensor's aperture close to the center of ion beam. The ion source aperture diameter is 36 mm.

The beam intensity can be measured by the Faraday cup, which could be turned to close the aperture. Different ways to set the beam are possible:

- to make the parallel ion beam
- to defocus beam slightly. The beam size is limited by the aperture size which is positioned at the distance approximately $1.8m$ far from the ion source. So the maximum divergency of the defocused beam is less than 2%. That gives the ion beam spot at the NPD position about $60mm$ in diameter as maximum. An advantage of this method is that it is less time consuming.

The next conditions are applied during NPD calibration:

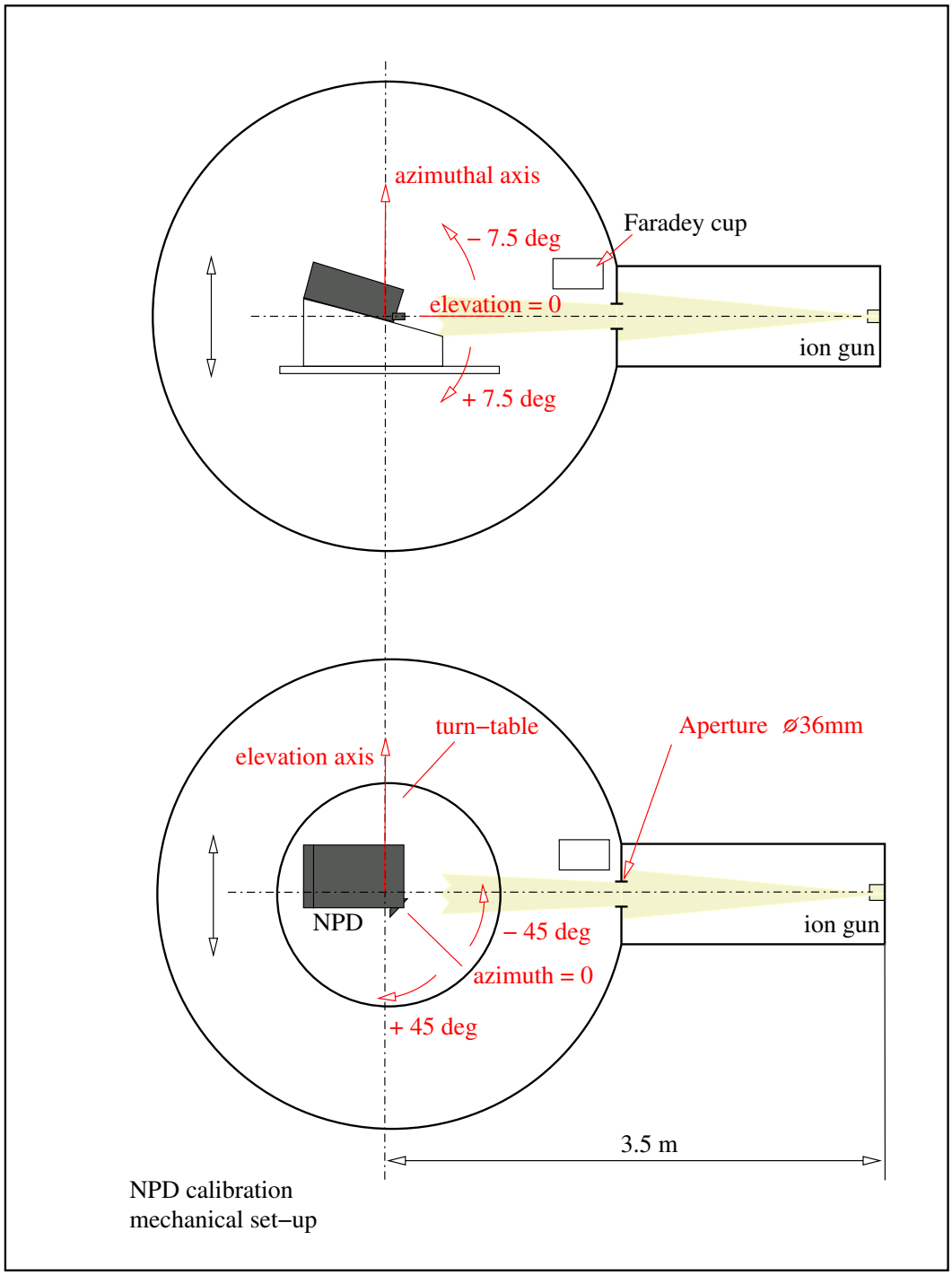

Figure 4: NPD calibration mechanical set up.

- Beam intensity in general case is set to keep a count rate on the StartMCP equal to $(1 \div 3) \times 10^3$ count/sec.
- Integration time: over 1 sec
- Deflector electrodes are grounded. So the sensor is calibrated using the charged ion beam. It is done to provide the proper beam current. Note: the neutral part of the ion beam is about a few procent of the initial beam current. The results are comparable to the measurements with ENA beam.
- The pressure in the vacuum chamber was kept approximately $4 \times 10^{-7} mbar$

1.4 Calibration plan

In order to get the relative and absolute characteristics of the instrument the next calibration procedure has been developed:

1. Saturation curve for MCPs. Nominal bias.
   Beam species: H_2O^+, Energy: 5keV
2. Angular response. Beam species: H^+, Energy: $5keV$
3. ToF spectra, PHd spectra analysis.
4. Energy and Mass identification
5. Efficiency.
   Beam Energy: 5.0 keV, 3.0 keV, 1.3 keV, 0.7 keV, 0.5 keV
   Species: H^+, H_2O^+
   Direction: Dir0, Dir1, Dir2
6. Geometrical Factor calculation
7. Heater. Temperature sensor.
8. Noise of the integrated instrument with ASPERA-3

2 Calibration of the NPD 2 Flight Model

2.1 MCP characterization.

To find out the nominal bias for all detectors characterization of MCP has been done under the next conditions. (The standard NPD configuration is used.)

- Ion beam:
  - Species: H_2O^+ ions
  - Energy: $5KeV$
  - Intensity: Beam intensity is taken so to keep count rate on StartMCP equal to $\sim 1 \div 3 \times 10^3$ count/sec.
- The MCP bias was increased from 2.3 kV to 2.85 kV by steps 50 V.
- Output: The count of Start and STOP events counters without correlation.
- Integration time: $\sim 1sec$

Figure 5 shows the count rate dependency on MCP bias of Stop0, Stop1, Stop2 detectors, bottom panel - of Start detector. The nominal bias corresponds to the saturation plateau of the count rate function.

MCP count rate saturates after 2700V on STOP MCPs and 2650V on StartMCP. Therefore nominal working bias is set to 2750V for all NPD detectors. START and STOP MCP bias are to be equal.

To compensate MCP gain degradation (if that occurs) the bias can be increased by al least 200V.

2.2 Angular response of NPD sensor

Figures 6, 7, 8 shows the angular response of each detector: Stop0, Stop1, Stop2. The upper left panel shows the measured 2D response. The upper right panel is the pictorial rendition of the 2D response. The left bottom panel shows the azimuthal response integrated over the elevation angle. The bottom right panel shows the elevation response integrated over the azimuthal angle.

The experimental results have been obtained for the following conditions:

- The incident beam species: H^+
- The beam Energy: $5KeV$
- Azimuthal scan: from -50° to $+50^\circ$ with step 5°
- Elevation scan is from -7.5° to $+7.5^\circ$ with step 1.5°
- Exposition: ~ 1 sec in each point

During calibration the valid count rate is measured. Valid count rate stands for the count of any StartMCP signal which is followed by a one of Stop detectors signal within the definite time window.

The surfaces fitting to be done.

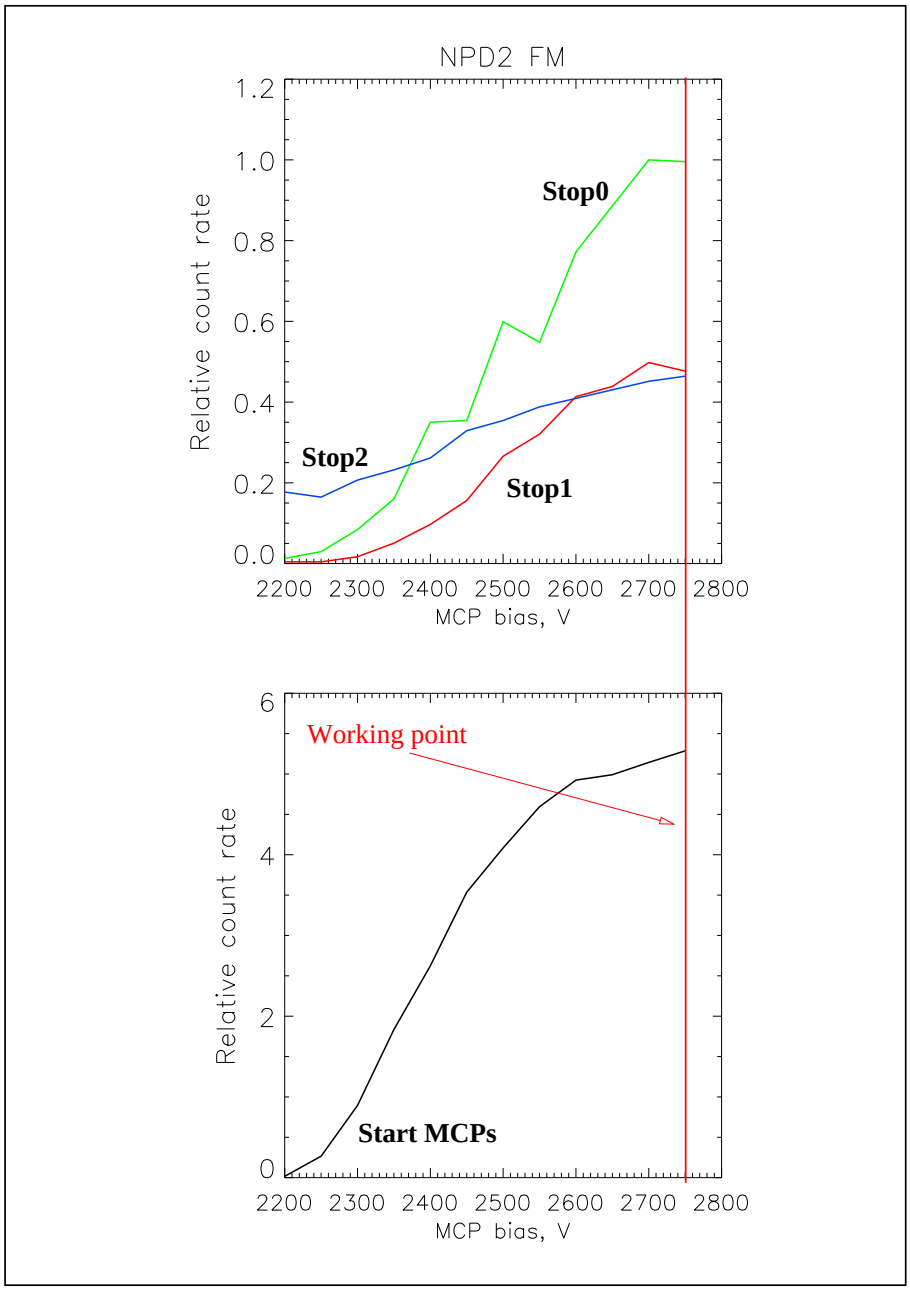

Figure 5: The upper panel shows the count rate dependency on MCP bias of Stop0, Stop1, Stop2 detectors, bottom panel - of Start detector. The nominal bias corresponds to the saturation plateau of the count rate function.

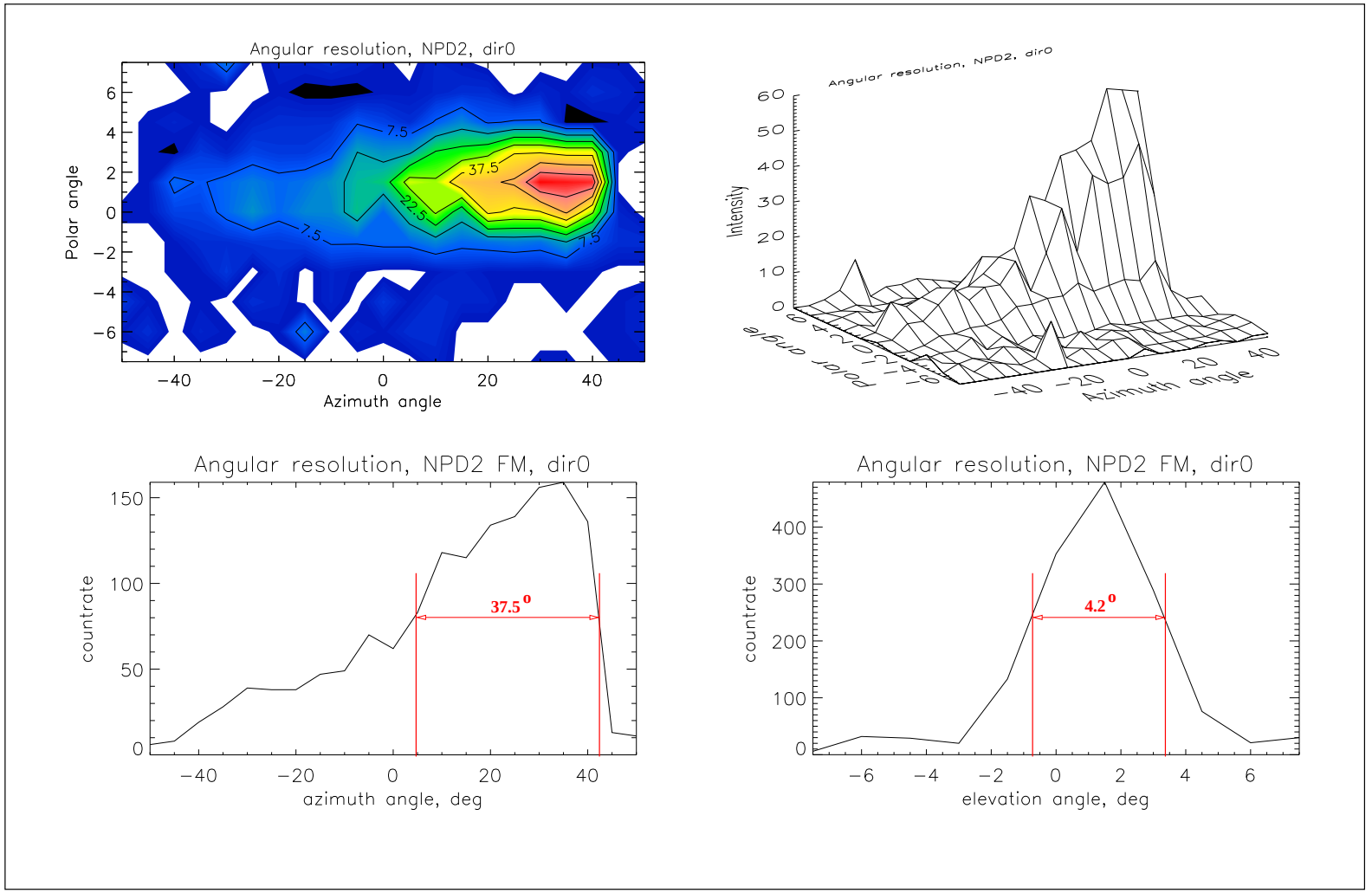

Figure 6: Angular response of the NPD sensor detector Stop0. The upper left panel shows the measured 2D response. The upper right panel is the pictorial rendition of the 2D response. The left bottom panel shows the azimuthal response integrated over the elevation angle. The bottom right panel shows the elevation response integrated over the azimuthal angles.

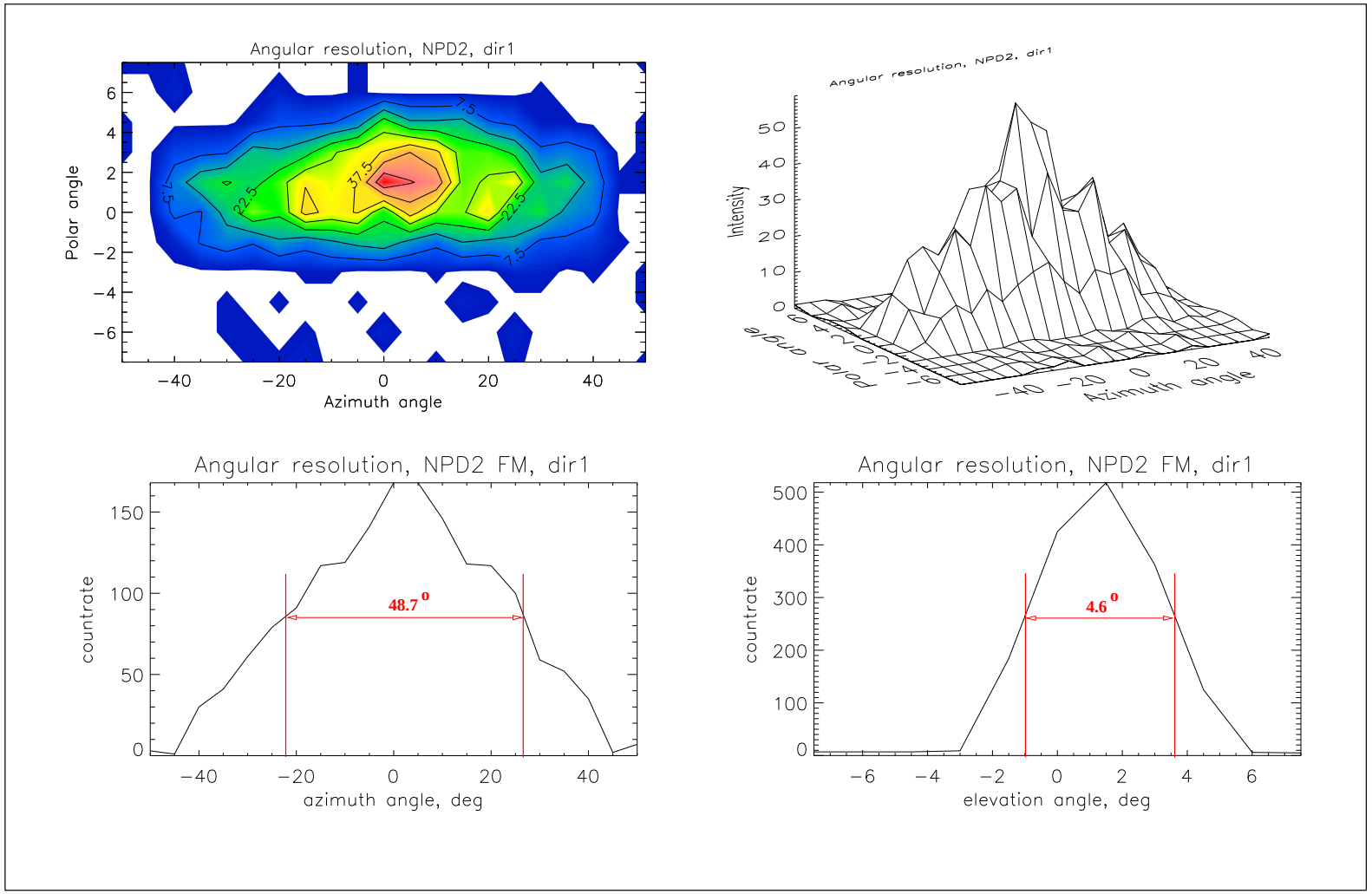

Figure 7: Angular response of the NPD sensor detector Stop0. The upper left panel shows the measured 2D response. The upper right panel is the pictorial rendition of the 2D response. The left bottom panel shows the azimuthal response integrated over the elevation angle. The bottom right panel shows the elevation response integrated over the azimuthal angles.

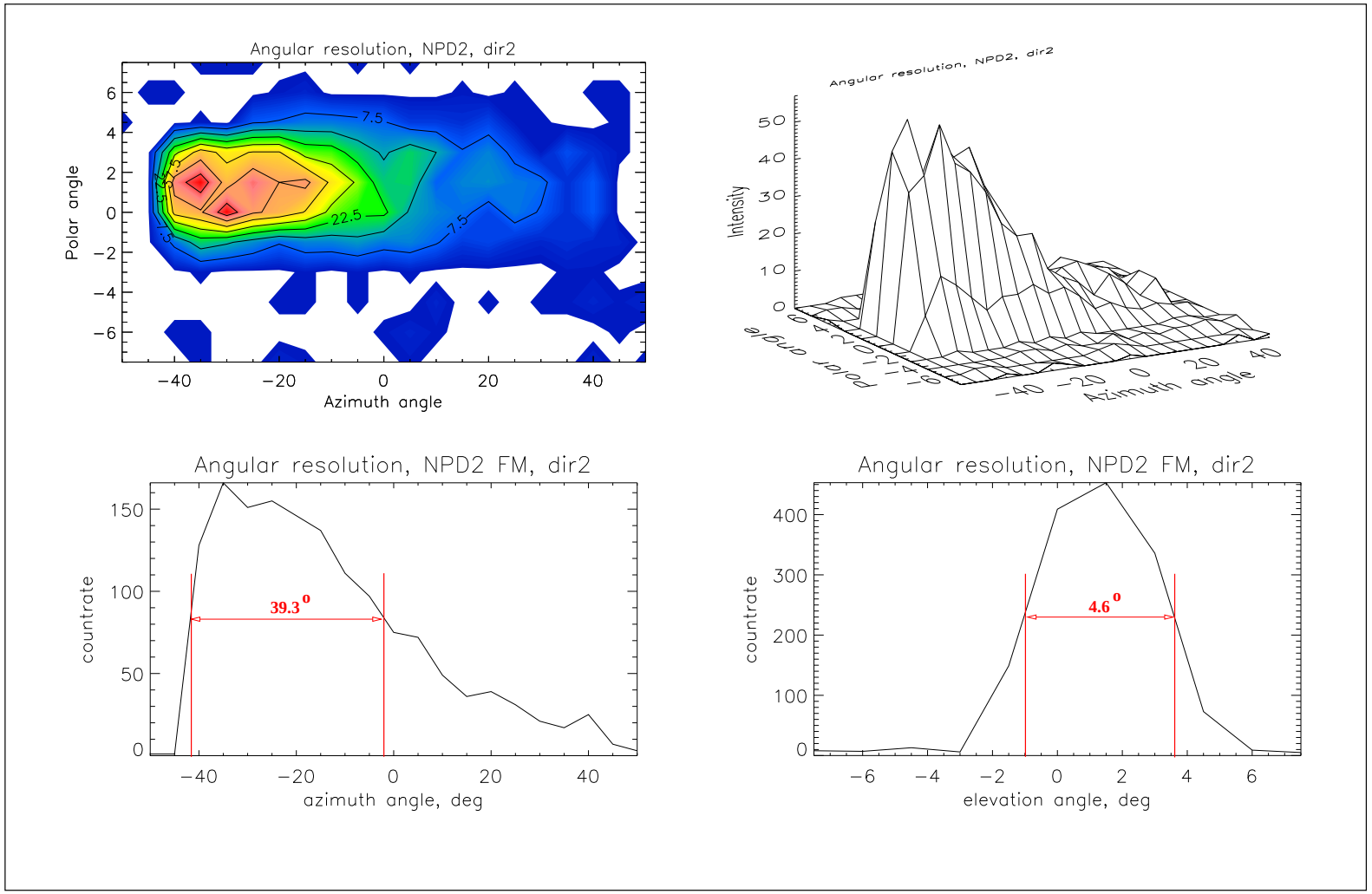

Figure 8: Angular response of the NPD sensor detector Stop0. The upper left panel shows the measured 2D response. The upper right panel is the pictorial rendition of the 2D response. The left bottom panel shows the azimuthal response integrated over the elevation angle. The bottom right panel shows the elevation response integrated over the azimuthal angles.

Figure 9 (upper panel) shows the azimuthal response of each detector (black curves) and the net response of the NPD sensor (red curve). The bottom panel shows the elevation response of each detector (black curves) and the net response of the NPD sensor (red curve).

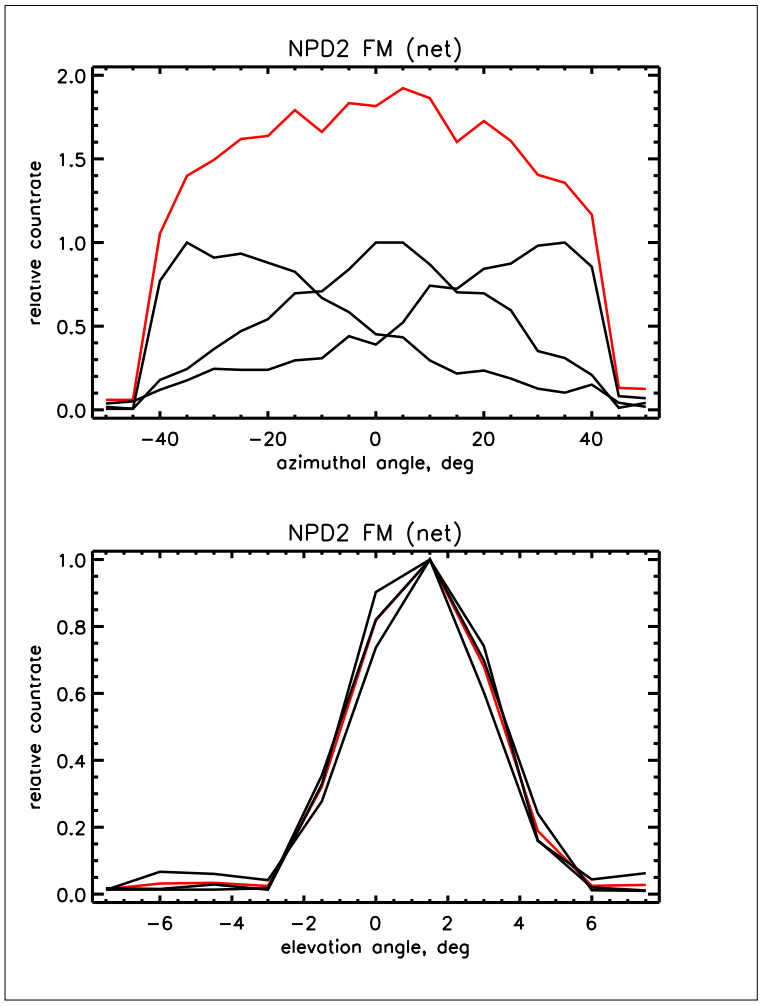

Figure 9: The sensor's angular response for each direction and overall the detectors.

Despite the fact that curves over-crosses each other, it is possible to resolve an incoming beam direction by comparing the count rate of detectors. The detector with larger count rate shows an incident beam direction. The FWHM of the curves is wider in comparison to the theoretical calculations. That can be explained by the properties of the Start surface. The Stop0 and Stop2 detectors peaks are limited at the outer sides, that could be due to the geometrical position and shape of the baffles, placed between the Start Surface edges and the Stop surface edges. The elevation response curves are looking similar, because they are defined by the deflector configuration (position of deflector electrodes).

Finally the FWHM of both azimuthal and elevation responses are shown in the Table 1.

	Azimuthal response, deg	Elevation response, deg
$Dir0$	37.5	4.2
$Dir1$	48.7	4.6
$Dir2$	39.3	4.6
$overall$	81.8	4.5

Table 1: Table shows both azimuthal and elevation responses of all three detectors of NPD2 and the total response of NPD2 sensor

2.3 ToF spectra

There will be examples of ToF spectra in both RAW and BIN modes.

2.4 PhD spectra

There will be examples of PhD spectra in both RAW and BIN modes.

2.5 Energy and Mass identification

2.5.1 Energy resolution

Figure 10 shows the TOF of particles dependency on the incident beam energy. The X-axis – is ion beam energy in log scale. The Y-axis – is particles ToF in log scale. On this plot the position of ToF peaks for the set of ion beam energies are plotted by color-coded dots. Error bars show the FWHM of ToF peaks. The lower line (blue) stands for H^+ ions and the upper line (red) stands for O^+ ions. This plot delineates TOF dependency on particles energy. Dots are sitting along the straight line. Therefore $\frac{\Delta E}{E} \approx$ const. That means that an ion velocity can be definitely calculated from its TOF. These curves can be expressed by the next equations:

$$E(H^+, Dir0) = A_0^0 + A_1^0 \cdot T^{-1} + A_2^0 \cdot T^{-2}$$

$$E(O^+, Dir0) = B_0^0 + B_1^0 \cdot T^{-1} + B_2^0 \cdot T^{-2}$$

$$E(H^+, Dir1) = A_0^1 + A_1^1 \cdot T^{-1} + A_2^1 \cdot T^{-2}$$

$$E(O^+, Dir1) = B_0^1 + B_1^1 \cdot T^{-1} + B_2^1 \cdot T^{-2}$$

$$E(H^+, Dir2) = A_0^2 + A_1^2 \cdot T^{-1} + A_2^2 \cdot T^{-2}$$

$$E(O^+, Dir2) = B_0^2 + B_1^2 \cdot T^{-1} + B_2^2 \cdot T^{-2}$$

where
E – ion particles energy, keV
T – ion particles ToF number, ns
A^i_j, B^i_j – coefficients
i – direction
j – coefficient number

A and B values to be calculated.

One of the important results can be formulated as follows: for the definite energy range (0.1 kev - 10 kev) low energy O^+ ions can be distinguished from the high energy H^+ particles by only the ToF values. On the plot (Figure 10) the functions overlap within the TOF window 280 ns – 590ns. So, the particles with ToF more than 590 ns are O^+ definitely. And the particles with ToF less than 280 ns are H^+ ions. Of course the energy of incoming heavy particles can be more than $10keV$, therefore the curves overlapping ToF window can be extended to lower values. The ions (both light and heavy) with ToF that fit that window have comparable velocities. So to distinguish between these species one has to analyze the PHD of the Stop detectors. In case of O^+ ion species of higher energy than 10 keV the estimation of particles mass based only on the TOF analysis is not very clear. For such cases the analysis of FWHM of ToF distribution can be used additionally to the PH analysis.

So we can use ToF analysis to resolve energy of ion species in such mass and energy range:

- O^+ ions
  E < 2.8 keV
  ToF > 590 ns

- H^+ ions
  E > 0.7 keV
  ToF < 280 ns

And we have to use the PH analysis for ions species with ToF that fit the TOF window $280ns$ – $590ns$ and are within the next mass and energy range:

- TOF window: 280 ns – 590 ns
- $E(O^+)$ = 2.8 KeV – less 10 KeV
- $E(H^+)$ = 0.1 keV – 0.7 keV

By the way the lowest limit of light particles energy that can be measured by the NPD sensor is 0.1 keV. For the lower energy ions scattering on the StartSurface is too high.

By applying the numbers calculated above for the compressed mode data ToF window will have the next values:

- TOF window: 246 ns – 610 ns

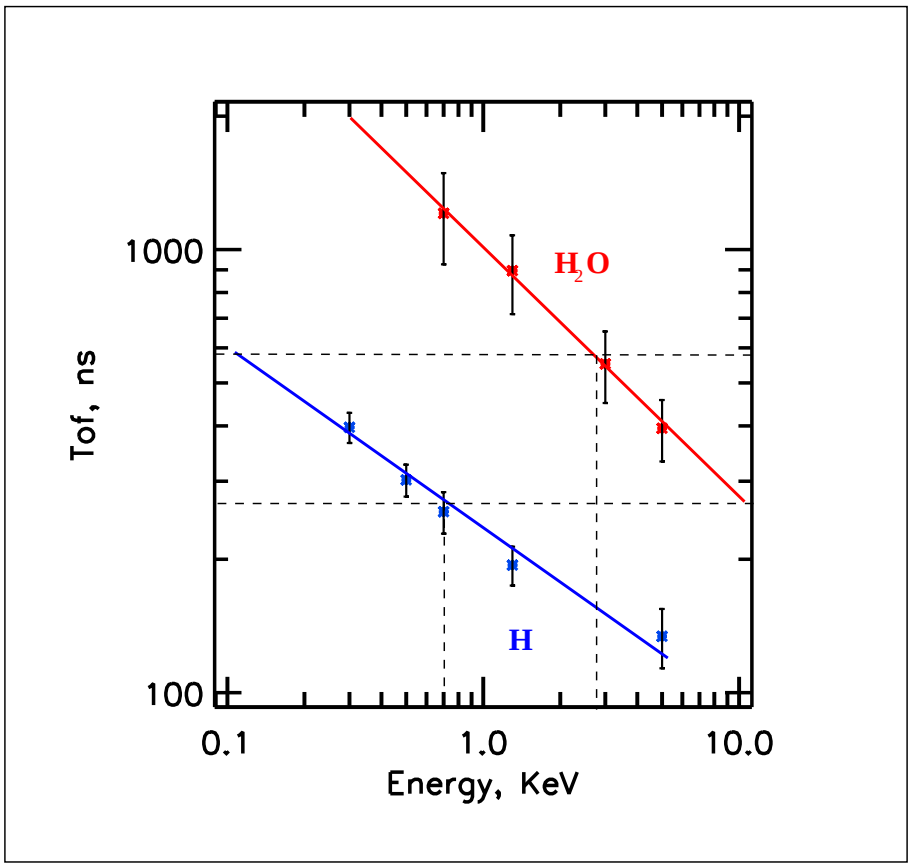

Figure 10: The figure shows the TOF dependency on beam energy of different ion species (H^+, O^+) for direction 1

- ▷ Compressed mode: 7 – 10 steps
- ▷ $E(O^+)$ = 2.4 KeV – less 11 KeV
- ▷ $E(H^+)$ = 0.1 keV – 1.0 keV

ToF step 7 (compressed mode) consists of 246–309 ns ToF interval
ToF step 10 (compressed mode) consists of 486–610 ns ToF interval

2.5.2 Mass resolution

Particles with different masses and the same velocity produce different amount of secondary electrons while hit the StopSurface and sensor's front end electronics produces the corresponding output analog signal. The heavier ions produce the larger number of secondary electrons

from the STOP surface than the lighter ones and therefore electronics produces the output analog signal of higher magnitude. The amplitude (pulse height) of that output signal is analyzed then. A 8-bit output signal can be scaled according to the Raw Data table from 0 to 255 levels, where 255 level corresponds to the maximum signal, and according to the Compressed Data table from 0 to 15 levels, where level 15 corresponds to the maximum signal. Level number is called channel number is terms of NPD electronics. The typical statistical Pulse Height distributions are presented on the Figure 11.

On the bottom panel PH distributions of detectors output signals produced by H^+ and O^+ particles of the same velocity are shown. Compressed mode data is used for analysis. The channel number is set on X-axis. Relative count rate is set on Y-axis.

Analysis of PH distributions shows that low energetic lighter H^+ ions produces output PH signal of lower amplitude, that give short tail peak in terms of PH distribution. Meanwhile heavier O^+ ions produces output PH signal of higher amplitude, that give long tail peak in terms of PH distribution. On the plot the H^+ peak ends at the channel number 9. But the O^+ peak has a long tail. Assuming the criteria that H^+ peaks have a largest channel number equal to some channel number less than 15 (in our case it is 9), conclude that a longer peak tail (channels 10–15) is created by only O^+ ions. Let's mark the end of H^+ peak slope on the bottom panel by setting a threshold. To calculate the O^+ peak tail one has to integrate the area on the right hand of this PH threshold. Let me define a PH threshold by X. Again, in our case here X = 9.

The integral of an O^+ peak tail area S_O^t:

$$S_O^t = \sum_{i=X}^{15} C(i) \tag{1}$$

where
i – the number of channel, 0,1,...,15
C(i) – a number of pulses with an amplitude i
X – PH threshold

and the integral of an O^+ peak full area S_O:

$$S_O = \sum_{i=0}^{15} C(i)$$

Then calculate the ratio K between an O^+ peak full area and an O^+ peak tail area.

$$K = \frac{S_O}{S_O^t}, \tag{2}$$

where
S_O^t - integral of the O^+ peak tail area

S_O - integral of the O^+ peak full area

The upper panel of Figure 11 presents the sum of the H^+ and O^+ peaks, superposed on the bottom panel. The black line shows the total peak. The red line shows the O^+ part of the total peak. In general case it will be necessary to split such netpeaks into H^+ and O^+ peaks. Using the calculated coefficient K, we can calculate the part of O^+ peak in the sum peak. Then H^+ peak part can be calculated by extracting the O^+ peak area from the sum peak area.

The integral of a $O^+ + H^+$ total peak full area S is:

$$S = \sum_{i=0}^{15} C(i) \tag{3}$$

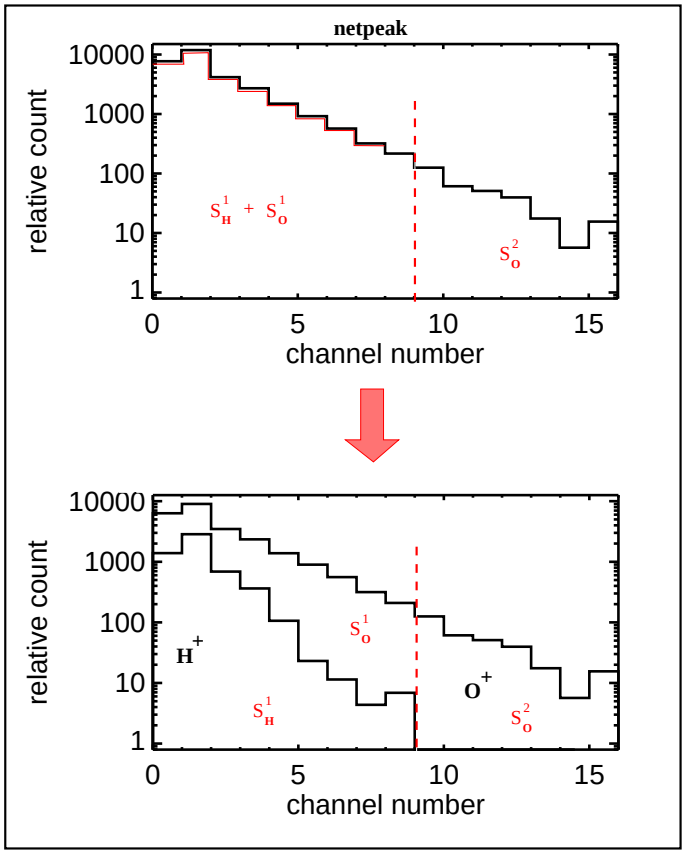

Figure 11: The bottom panel shows the PH distribution of H^+ species and O^+ species with the same particles velocity. The upper panel presents the sum of the H^+ and O^+ peaks, superposed on the bottom panel. The black line shows the total peak. The red line shows the O^+ part of the total peak.

And O^+ peak area is:

$$S_O = S_O^t \times K \tag{4}$$

where

S_O^t – O^+ peak tail area can be calculated by equation 1

K – constant, calculated during detector calibration (equation 2)

Then a H^+ peak area is:

$$S_H = S - S_O \tag{5}$$

where
S_H – H^+ peak area integral
S – $(O^+ + H^+)$ sum peak full area integral
S_O – O^+ sum peak full area integral

The calculation of the weights of O^+ and H^+ in the total peak procedure can be developed also by taking into account the H^+ peak tail area.

Figure 12 shows the Pulse Height distribution for H^+ (on the left hand) and O^+ (on the right hand) ion species of the same particles velocity of all detectors. The upper panels show the detector Dir0 PH response, the middle panels show the detector Dir1 PH response and the bottom panels correspond to the detector Dir2 response.
Finally the thresholds settings for all detectors are shown in the Table 2. Also the coefficient K numbers for each detector are in that table. The thresholds and ratio coefficients values can be recalculated later for taking into account MCP degradation, STOP surface properties changing and PH distribution shape change as a result.

NPD 2 FM		
	Threshold X	K
$Dir0$	12	15.8
$Dir1$	9	78.6
$Dir2$	11	12.9

Table 2: Table shows the thresholds for all detectors and the ratio between an O^+ peak full area and an O^+ peak tail area coefficients K.

2.5.3 Some technical details.

NPD is programmed to produce the ToF values within the next range: $50ns$ – $1500ns$. The lower border is set so to cut off the electron ToF peak data. By the higher border the region of interest is defined. Let's take a look at the valid data of NPD sensor. Valid data means the

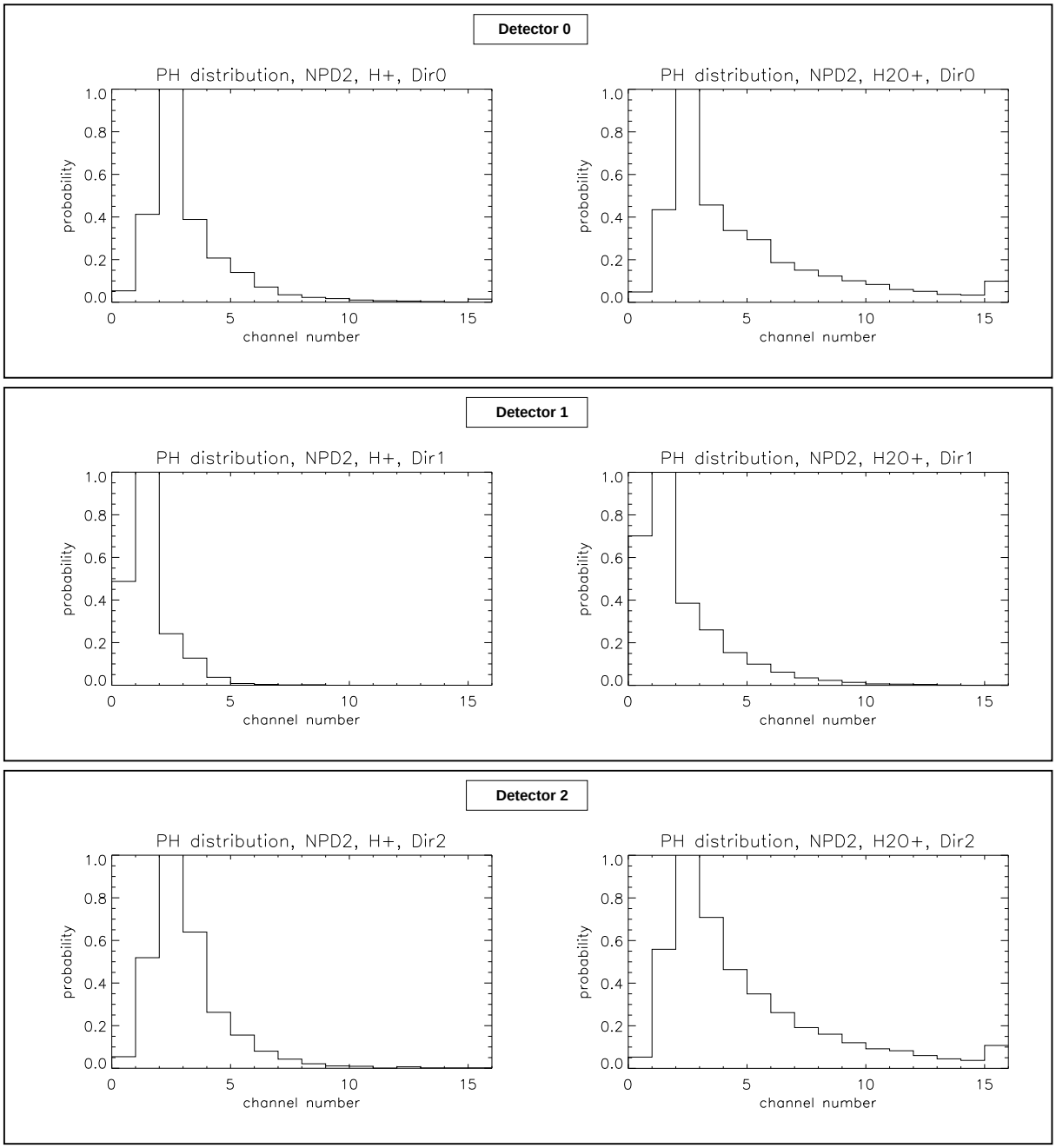

Figure 12: The figure shows the PH distribution for H^+ species (left panel) and O^+ species (right panel) of the same particles velocity for each NPD detector.

event when any signal on one of the 3 Stop detectors corresponds to one signal on Start detector, within the defined TOF window $50ns - 1500ns$. DigTOF electronics sets the $coin$cidence flag equal to 1 for events of such type.

'BINning Array' mode data presents an array of compressed according to special algorithm valid data, both PH and TOF numbers. This data is fitted info the matrix $16 \times 16 \times 3$, $[ToF \times PH \times Dir]$.

Uncompressed TOF event data is a number between $1ns$ to $1500ns$. In compressed form — number in-between $0 - 15steps$. Uncompressed PH data has numbers between 1 to 255 steps. Compressed numbers — in-between $0 - 15steps$

Binning data array is a matrix 16x16x3 with COIN flag = 1. It consists of:

- 16 TOF steps
- 16 PH steps
- 3 Directions

RAW mode would be used for calibrations and to get TOF mode. The main working mode would be Binning mode.

Here will be ToF mode description

2.5.4 ToF-PhD matrix

Let's take a matrix 16×16 for direction Dir1 (for example) and plot it in the next coordinates: ToF values at X-axis, PhD values at Y-axis. Then set the TOF window borders for compressed mode data specified at the *Energy resolution* section. These vertical borders include ToF steps 7 and 10. Left border separates event counters of less than 7 step, right one separates TOF events counters of the step more than 10. All data on the left hand (0 – 6 steps) corresponds to H^+ ions events, all data on the right hand (11 – 15 steps) corresponds to O^+ ion events.

Then set the PH threshold for that direction detector calculated in the previous *Mass resolution* section. To distinguish between ion species within the TOF window 7-10 steps the PH analysis in compressed mode is used. So the threshold here is set to 9.

Finally to analyze particles mass and energy, TOF-PHD matrix based on the the detector Dir1 data has been built, see Figure 13. The black thick line separates two regions of the matrix. The part of the matrix on the left hand corresponds to H^+ ions and the part of it on the right hand corresponds to heavy O^+ ions.

2.6 Efficiency

NPD sensor efficiency depends on a set of factors like ion beam species mass and energy, MCP bias voltage, azimuthal and elevation angles, so on. To measure the sensor's absolute efficiency the next conditions should be fulfilled:

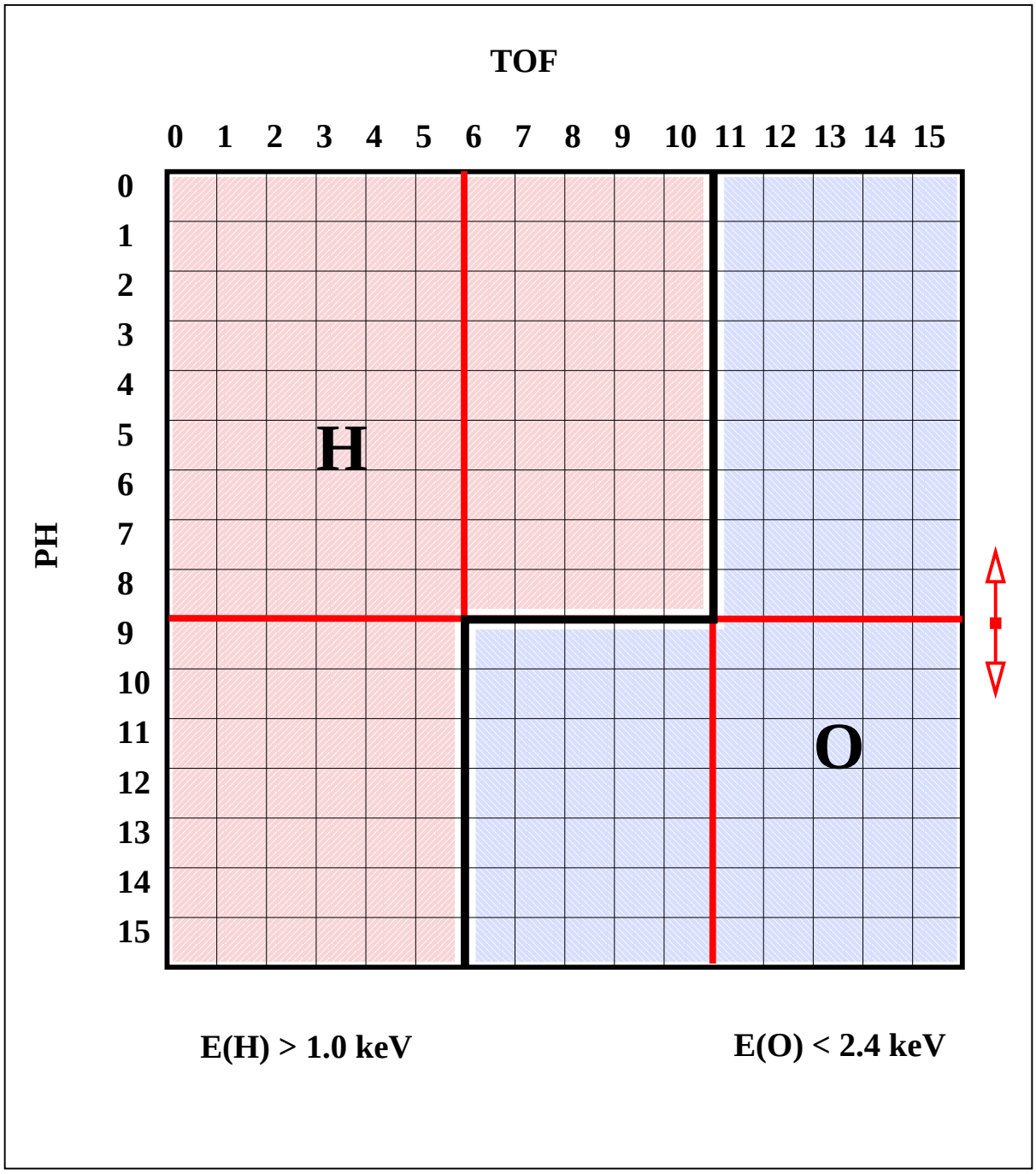

Figure 13: TOF-PHD matrix based on the the detector Stop1 data, built to analyse ion particles mass and energy.The black thick line separates two regions of the matrix. The part of the matrix on the left hand corresponds to H^+ ions and the part of it on the right hand corresponds to heavy O^+ ions.

- Count rate measurement at α_0, β_0 - angles at which the detectors count rate has a maximum value.
- Ion beam is parallel and stable
- Ion beam spatial distribution is homogeneous.
- MCP bias voltage is stable.

The default position of NPD sensor during efficiency measurements is α = 0, β = 0. But as it is seen from angular response measurements, the maximal count rate is achieved at β_e = $1.5°$. The ratio between detector's count rate at α, β: C(α, β) and count rate at α, β_e: C(α, β_e) is K_e:

$$K_e = \frac{C(\alpha, \beta_e)}{C(\alpha, \beta)}$$

where
K_e - elevation coefficient

The efficiency values are to be corrected by using the K_e coefficient.

Measurements by the detector Dir1 are performed at $\alpha = 0°$. Measurements by the detectors Dir0 and Dir2 are performed at $\alpha = +/-40°$(see Figure 4). For the azimuthal angle α equal to $45°$, count rate drops drastically (see Figure 9). The maximum azimuthal response is achieved with the next α angles:

Dir0 α_a = $-35°$

Dir1 α_a = $0°$

Dir2 α_a = $+35°$

The ratio between detector's count rate at α, β: C(α, β) and count rate at α_a, β: C(α, β) is K_a:

$$K_a = \frac{C(\alpha_a, \beta)}{C(\alpha, \beta)}$$

where
K_a - azimuthal correction coefficient

The efficiency values are to be corrected by using the K_a coefficient also.

The table 3 shows the values of elevation and azimuthal correction coefficients for each of NPD detectors.

To minimize the ion beam not uniform spatial distribution effect on efficiency measurements all ion beam particles have been counted by performing the scan of the area larger than the ion beam spot at the NPD place. Scan procedure is shown on Figure 14. First of all by scanning along x-axis and/or y-axis beam borders had been found. Meanwhile it was checked if beam

	K_e	K_a
$Dir0$	1.37	1.1
$Dir1$	1.20	1.0
$Dir2$	1.12	1.2

Table 3: Table shows the values of elevation and azimuthal correction coefficients for each of NPD2 detectors.

is homogeneous. Beam could be adjusted if necessary. Sensor was displaced along the vertical and horizontal axes by steps dV = 3.0mm, dH = 4.5mm. Pinhole zigzagged covering the area A equal to:

$$A = 60 \times 63mm^2$$

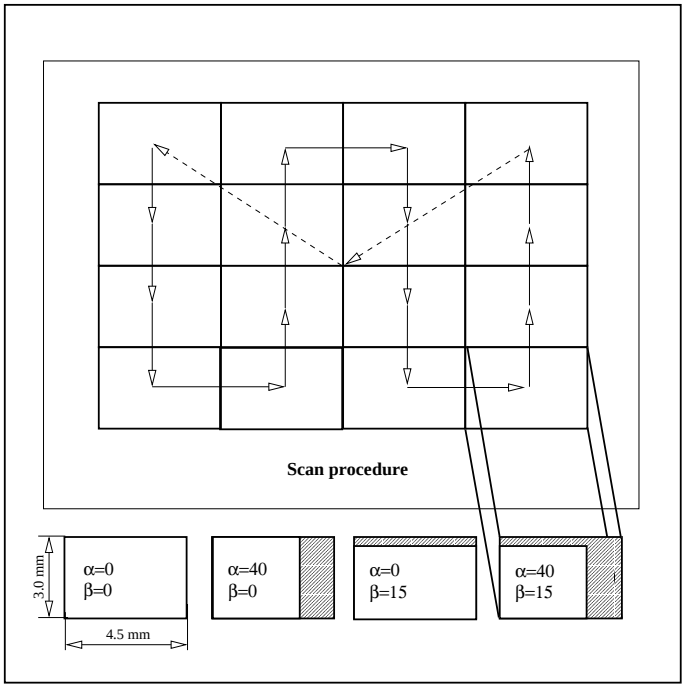

Figure 14: The upper figure shows a scan procedure for NPD sensor during calibration. The bottom figures show the pinhole open area in dependency on azimuthal and elevation angles.

Pinhole should cover whole beam area, therefore steps are chosen according to the pinhole sides lengths. This is valid for all directions. The integration time at each point is over 1 sec. Figure 15 shows the number of beam profile images got by the instrument for different ion masses and energy by sensor's detector Dir1. Finally the integral count rate is calculated. Also beam intensity has been checked before and after each scan. If beam intensity values differed then arithmetic mean was taking into account. Then efficiency has been calculated according to

the formula:

$$E_0 = \frac{C \cdot q_e \cdot T_{int}}{J} \tag{6}$$

where
E_0 - efficiency,
C - measured integral count rate, $\frac{1}{sec}$
q_e - electron charge,
T_{int} - integration time, s
J - beam intensity, A

Also it is necessary to take into account the pinhole area during measurements. The pinhole area dependency on the azimuth and elevation angles is shown on the Figure 14 lower panel.

- NPD is elevated on 15° => the pinhole area is decreased by $K_1 = \frac{1}{\cos 15^\circ}$
- For α=+/-40° pinhole area is decreased by $K_2 = \frac{1}{\cos 40^\circ}$. For $\alpha = 40^\circ$ scan steps should not be changed, but we have to take into account covered pinhole area coefficient K_2 to maintain the scan procedure. Otherwise it would take 2 times more steps for each scan, therefore 2 times longer. In that case beam intensity long-time variations can take place.
- Real integration time is $0.892sec$. That gives a time correction coefficient K_t:

$$K_t = \frac{1}{0.892} = 1.121$$

Finally the corrected efficiency formula is shown by Equation 7

$$\varepsilon = E_0 \cdot K_{meas} \tag{7}$$

where
ε – the corrected absolute efficiency of a detector
K_{meas} – efficiency correction total coefficient (equation 8)

$$K_{meas} = K_e \cdot K_a \cdot K_1 \cdot K_2 \cdot K_t \tag{8}$$

where
K_t - timing coefficient,
K_1 - declination coefficient 1/cos (14),
K_2 - (optional) pinhole open area coefficient for side directions,
K_e - elevation correction coefficient
K_a - azimuthal correction coefficient

The efficiency measurements has been done for the next ion beam settings:

- Energy: $5.0keV, 3.0keV, 1.3keV, 0.7keV, 0.5keV, 0.3keV$

- Mass: H^+, H_2O^+

In the Table 4 the coefficients K_{meas} and calculated final absolute efficiencies of all sensor's detectors are presented.

Figure 16 shows the NPD2 FM absolute efficiency in dependency on ion beam species mass and energy for all detectors.

Table 4 and the figure 16 to be updated by using K_e, K_a

Absolute efficiencies had been calculated using BINning array data (coincidence flag equal to 1).

NPD 2 FM							
	E, KeV	5.0	3.0	1.3	0.7	0.5	0.3
K_{meas}							
H_2O^+	Stop0	1.51	1.51	1.51	1.58	1.58	1.51
	Stop1	1.155	1.155	1.155	1.155	1.155	1.155
	Stop2	1.51	1.51	1.51	1.61	1.61	1.51
H^+	Stop0	1.51	1.51	1.51	1.58	1.51	1.51
	Stop1	1.155	1.155	1.155	1.155	1.155	1.155
	Stop2	1.51	1.51	1.51	1.61	1.51	1.51
$Efficiency, \%$							
H_2O^+	Stop0	$5.9 \cdot 10^{-2}$	$3.7 \cdot 10^{-2}$	$1.2 \cdot 10^{-2}$	$--\cdot 10^{-2}$	$--\cdot 10^{-2}$	$2.8 \cdot 10^{-4}$
	Stop1	$6.57 \cdot 10^{-2}$	$4.9 \cdot 10^{-2}$	$1.7 \cdot 10^{-2}$	$4.7 \cdot 10^{-3}$	$2.0 \cdot 10^{-3}$	$2.0 \cdot 10^{-4}$
	Stop2	$7.04 \cdot 10^{-2}$	$4.04 \cdot 10^{-2}$	$1.52 \cdot 10^{-2}$	$--\cdot 10^{-2}$	$--\cdot 10^{-2}$	$1.7 \cdot 10^{-4}$
H^+	Stop0	$3.1 \cdot 10^{-2}$	$3.1 \cdot 10^{-2}$	$1.8 \cdot 10^{-2}$	$--\cdot 10^{-2}$	$5.5 \cdot 10^{-3}$	$1.6 \cdot 10^{-3}$
	Stop1	$3.5 \cdot 10^{-2}$	$3.3 \cdot 10^{-2}$	$2.1 \cdot 10^{-2}$	$1.2 \cdot 10^{-2}$	$7.0 \cdot 10^{-3}$	$2.5 \cdot 10^{-3}$
	Stop2	$3.75 \cdot 10^{-2}$	$3.74 \cdot 10^{-2}$	$2.24 \cdot 10^{-2}$	$--\cdot 10^{-2}$	$6.5 \cdot 10^{-3}$	$2.2 \cdot 10^{-3}$

Table 4: Table shows the NPD2 efficiencies for different ion species and energies, for all detectors

The efficiency curves can be described by the next equations:

$$\varepsilon(H^+, Dir0) = C_0^0 + C_1^0 \cdot T^{-1} + C_2^0 \cdot T^{-2}$$

$$\varepsilon(O^+, Dir0) = D_0^0 + D_1^0 \cdot T^{-1} + D_2^0 \cdot T^{-2}$$

$$\varepsilon(H^+, Dir1) = 3.82 - 2.33 \cdot T^{-1} + 0.38 \cdot T^{-2}$$

$$\varepsilon(O^+, Dir1) = D_0^1 + D_1^1 \cdot T^{-1} + D_2^2 \cdot T^{-2}$$

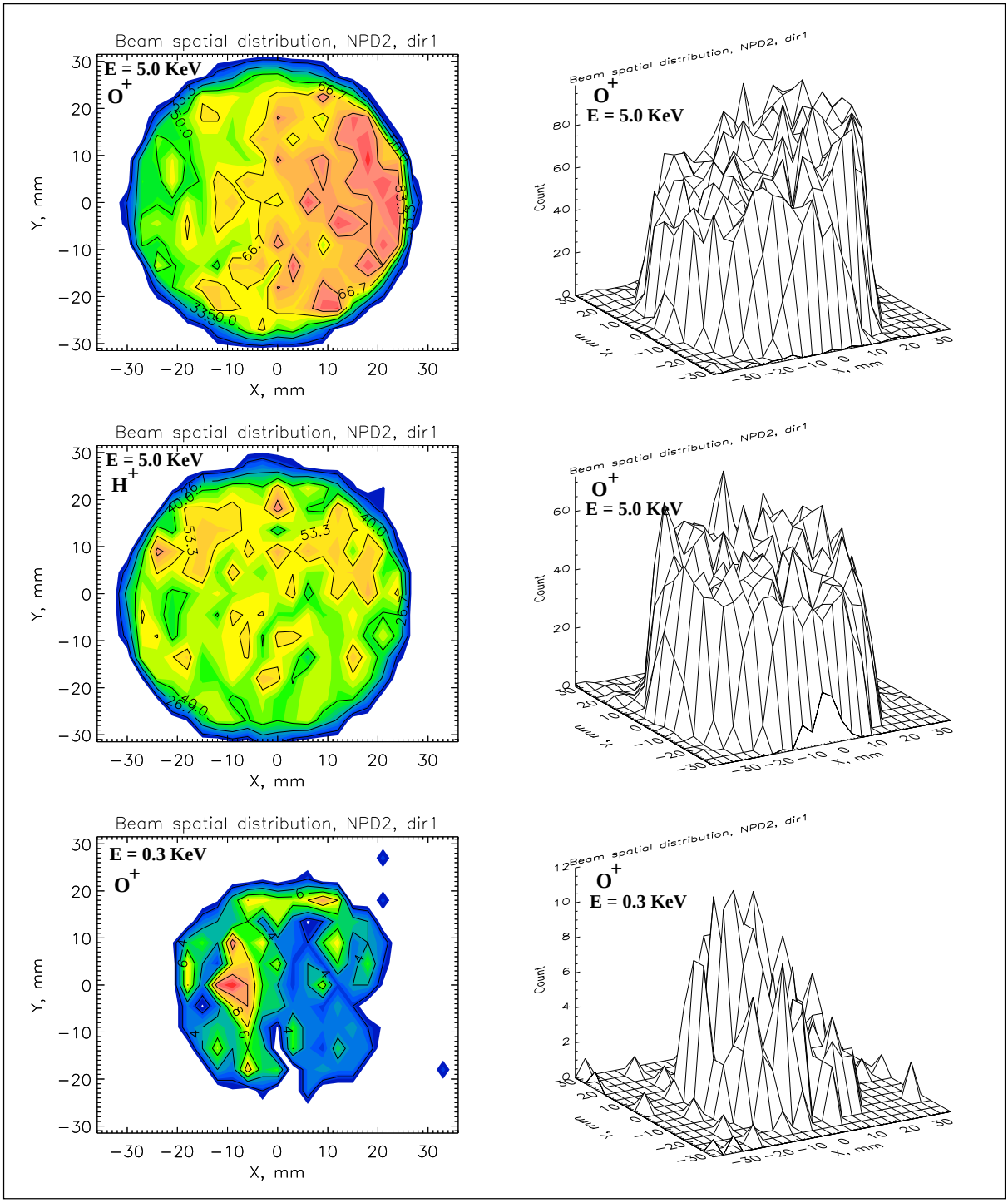

Figure 15: The figure shows the beam images as its are seen by NPD sensor.

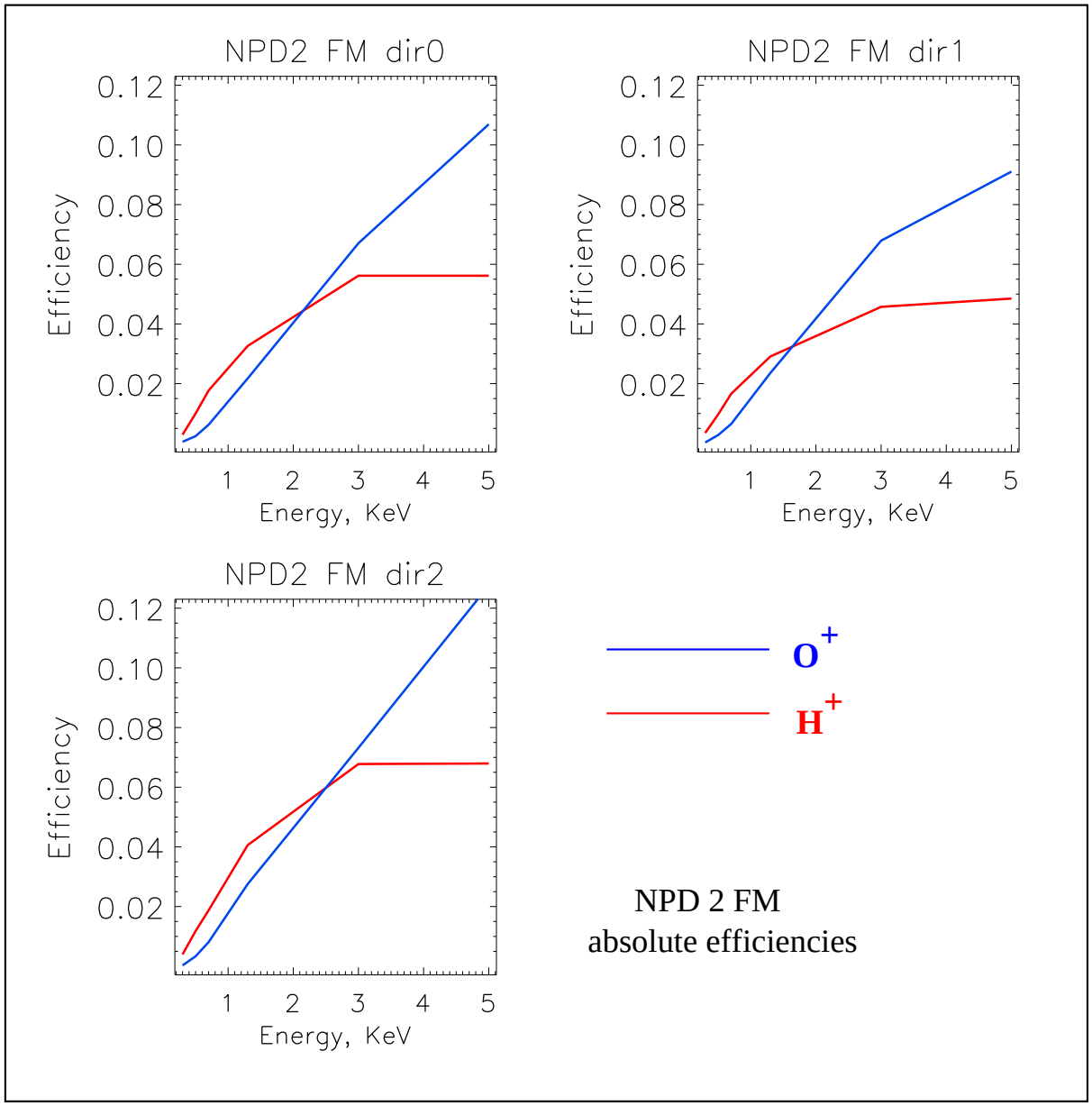

Figure 16: The figure shows the absolute efficiency of NPD2 sensor detectors in dependency on incident beam ions mass and energy.

$$\varepsilon(H^+, Dir2) = C_0^2 + C_1^2 \cdot T^{-1} + C_2^2 \cdot T^{-2}$$
$$\varepsilon(O^+, Dir2) = D_0^2 + D_1^2 \cdot T^{-1} + D_2^2 \cdot T^{-2}$$

where
ε – detector efficiency
E – ion particles energy, keV
C_j^i, D_j^i – coefficients
i – direction
j – coefficient number
C and D values to be calculated.

2.7 Geometrical Factor calculation

Geometrical factor of the instrument is an integral of the entrance effective area over solid angle as shown by Equation 9.

$$G = \int_\theta \int_\varphi A_{eff}(\theta, \varphi) cos\theta d\Omega \tag{9}$$

In our case that formula looks as below (Eq. 10):

$$G = \int_\alpha \int_\beta A_{eff}(\alpha, \beta) cos\alpha d\alpha d\beta \tag{10}$$

where
$A_{eff}(\alpha, \beta)$ - effective area of the sensor's aperture, depends on both azimuthal and elevation angles
α - azimuthal angle, deg
$d\alpha$ - displacement in an azimuthal plane, deg
β - elevation angle, deg
$d\beta$ - displacement in an elevation plane, deg

Effective area of a sensor's aperture is a measured count rate over ion beam density

$$A_{eff}(\alpha, \beta) = \frac{C(\alpha, \beta)}{P} \tag{11}$$

where
$C(\alpha, \beta)$ - sensor count rate (depends on azimuthal and elevation angle)
P - ion beam density, $\left[\frac{1}{cm^2 sec}\right]$,

P can be expressed by ion beam current measured by a Faraday cup and ion source aperture area (Eq. 12)

$$P = \frac{J}{q_e \cdot S_s \cdot t} = \frac{C_s}{S_s}, \tag{12}$$

$q_e = 1.6\times10^{-19}C$
J – Faraday cup current, A
S_s – ion source aperture area, cm^2
t – integration time, sec
C_s – ion source output count rate, $\frac{1}{sec}$

$$C_s = \frac{J}{q \cdot t}$$

Substitute A_{eff} for Equation 10

$$G = \int_\alpha \int_\beta \frac{C(\alpha,\beta)}{P} cos\alpha \cdot d\alpha d\beta \tag{13}$$

P – a constant, so it goes out of an integral sign. Let's divide and multiply the Equation 13 by $C(\alpha_0, \beta_0)$

$$G = \frac{C(\alpha_0,\beta_0)}{P} \int_\alpha \int_\beta \frac{C(\alpha,\beta)}{C(\alpha_0,\beta_0)} \cdot cos\alpha \cdot d\alpha d\beta \tag{14}$$

where
α_0, β_0 - azimuthal and elevation angles at which the count rate of a sensor is maximal for the corresponding detector,
$C(\alpha_0, \beta_0)$ – sensor's count rate, measured at the position (α_0, β_0)

Here an integral part of an equation 14 is a constant G_0 describing the angular properties of the sensor.

$$G_0 = \int_\alpha \int_\beta \frac{C(\alpha,\beta)}{C(\alpha_0,\beta_0)} \cdot cos\alpha \cdot d\alpha d\beta \tag{15}$$

Equation 15 shows a geometrical constant of the sensor. The geometrical factor equation looks now as follows:

$$G = \frac{C(\alpha_0,\beta_0)}{P} \cdot G_0 \tag{16}$$

Then I substitute the beam density P in Equation 13 by the formula 12

$$G = \frac{C(\alpha_0,\beta_0) \cdot S_s}{C_s} \cdot G_0 \tag{17}$$

Now let me set the sensor efficiency into geometrical factor calculation.
The sensor efficiency can be expressed by Eq. 18

$$\varepsilon = \frac{C(\alpha_0, \beta_0)}{C_s} \cdot \frac{S_s}{S_p} \tag{18}$$

where
S_p – sensors pinhole area
ε - detector's efficiency, calculated by Equation 6

Now ion source output count rate C_s at Equation 17 is to be substituted by the C_s expression from Equation 18. Finally,

$$G = G_0 \cdot S_p \cdot \varepsilon \tag{19}$$

Calculated geometrical constants of NPD2 detectors are presented in the table 5

	Dir0	Dir1	Dir2
G_O	0.0504	0.0604	0.0535

Table 5: Table shows the geometrical constants of all three detectors of NPD2

The table 6 shows the geometrical factor of the NPD sensor in dependency on incident ion beam energy and ion species mass.

NPD 2 FM $GeometricalFactor$							
E, KeV		5.0	3.0	1.3	0.7	0.5	0.3
H_2O^+	Stop0	$4.01 \cdot 10^{-4}$	$2.5 \cdot 10^{-4}$	$8.16 \cdot 10^{-5}$	$--\cdot 10^{-5}$	$--\cdot 10^{-5}$	$1.91 \cdot 10^{-6}$
	Stop1	$5.36 \cdot 10^{-4}$	$4.0 \cdot 10^{-4}$	$1.39 \cdot 10^{-4}$	$3.83 \cdot 10^{-5}$	$1.63 \cdot 10^{-5}$	$1.63 \cdot 10^{-6}$
	Stop2	$5.1 \cdot 10^{-4}$	$2.92 \cdot 10^{-4}$	$1.1 \cdot 10^{-4}$	$--\cdot 10^{-5}$	$--\cdot 10^{-5}$	$1.23 \cdot 10^{-6}$
H^+	Stop0	$2.11 \cdot 10^{-4}$	$2.11 \cdot 10^{-4}$	$1.23 \cdot 10^{-4}$	$--\cdot 10^{-5}$	$3.74 \cdot 10^{-5}$	$1.09 \cdot 10^{-5}$
	Stop1	$2.85 \cdot 10^{-4}$	$2.69 \cdot 10^{-4}$	$1.71 \cdot 10^{-4}$	$9.78 \cdot 10^{-5}$	$5.71 \cdot 10^{-5}$	$2.04 \cdot 10^{-5}$
	Stop2	$2.71 \cdot 10^{-4}$	$2.7 \cdot 10^{-4}$	$1.62 \cdot 10^{-4}$	$--\cdot 10^{-2}$	$4.69 \cdot 10^{-5}$	$1.59 \cdot 10^{-5}$

Table 6: Table shows the Geometrical factor dependency on ion species mass and energy.

2.8 Heater + temp. sensors

Temperature sensors are calibrated and tuned in ASPERA-3 instrument. Heater increases temperature of the START unit on 50 degrees in comparison with the ambient temperature.

Heating test has been done during calibration. Heater had been switched on for ≈10 hours. Measurements have been done before and after StartSurface heating. TOF distribution didn't vary after heating. That can be explained either by too short heating time period or by too low maximum temperature of StartSurface, reached during heating or by the StartSurface cleanness.

The temperature rising and falling curves will be presented here.

2.9 Noise

NPD electronics in its most sensitive state is sensitive enough to pick up the electric noise (even without MCP HV bias). So to decrease the electric noise level electronics' discriminators thresholds are set to maximum values, that level in binary form is 0×00 and corresponds to 5V on DAC.

During calibrations we used slightly different setup from the flight unit configuration. Therefore noise level is different between the laboratory setup and the flight one. Special actions have been done to decrease NPD sensors noise level in the Flight configuration of ASPERA-3.